Propulsion and Energy Forum
July 25-27, 2016, Salt Lake City, UT
52nd AIAA/SAE/ASEE Joint Propulsion Conference

Measurements and theory of driven breathing oscillations in a Hall effect thruster

Kentaro Hara *, Scott Keller †, and Yevgeny Raitses ‡
Princeton Plasma Physics Laboratory, Princeton, NJ, 08543

Breathing mode oscillations in Hall effect thrusters occur depending on the operation parameters such as discharge voltage, anode mass flow, and magnetic field. Time-dependent laser-induced fluorescence is used to measure the ion velocity distribution functions (IVDFs) with a modulating anode voltage. [Diallo et al. RSI 2015] Experimental results suggest that the IVDFs vanish or shifts its peak to a small velocity near the maximum peak of the discharge current oscillation. A zero-dimensional plasma global model [Hara et al. PoP 2014] is used to analyze the ionization oscillation mode by forcing the electric field to oscillate with a certain strength and frequency. In this model, the neutral atom continuity equation, the ion continuity and momentum equations, and electron energy equation are taken into account. Global model suggests that the ion mean velocity can fluctuate in time and is in-phase with the electric field oscillation. A 1D hybrid simulation shows that there can be a region where ion distribution exists in slow velocity (∼1000 m/s) due to reversed electric field during the oscillation.

I. Introduction

Breathing mode is a low-frequency ionization oscillation mode in the 5-30 kHz range that is widely observed in Hall effect thrusters (HETs). It has been experimentally observed that the breathing mode can stabilize depending on the operation parameters such as magnetic field, discharge voltage, anode mass flow, and cathode mass flow.[1–4] Several numerical simulations have also shown that breathing mode occurs in the HETs using both fluid and kinetic models.[5–9] However, the mechanism behind these ionization oscillations, specifically the direct source of what causes the excitation and stabilization, has not been identified. The most common theoretical explanation was that ions and neutral atoms undergo a natural oscillation mode, which is characterized by the Lotka-Volterra equations. This is often called the predator-prey model,[5] as the plasma behaves like a predator and neutral atoms are consumed as prey via the ionization process.

Sekerak et al. has extensively studied the ionization oscillation modes in the axial and azimuthal directions using a high-speed Langmuir probe and ultrafast imaging techniques.[4] The results showed that the fluctuation in the ion density is in-phase with the discharge oscillations. A hybrid kinetic/fluid model was used to investigate the mode transition by Hara et al.[9] in comparison to experiments. Numerical results suggest that electron transport and the heating/cooling mechanisms play an important role in stabilization and excitation of the breathing mode. In order to support the experimental and computational observations, a linear perturbation theory of ionization oscillations was developed by Hara et al.[10] First, the predator-prey model is revisited and shown to be insufficient. Next, ion and neutral atom continuity equations are formulated with more realistic terms, from which the mode is shown to be unconditionally damped. Finally, the perturbation in electron energy is added and positive growth rates are observed depending on the electron mean velocity and electron energy.

Laser-induced fluorescence (LIF) is a useful spectroscopy technique to obtain the velocity distribution functions (VDFs) of ions and neutral atoms. In this study, coherent breathing oscillations are driven by modulating the anode potential to validate time-resolving LIF developed by Diallo, Shi, and Keller.[11] One main advantage of a time-resolving LIF is that faster measurements of ion VDFs avoid thermal drifts. It

*Visiting Research Physicist, JSPS Postdoctoral Fellow, Princeton Plasma Physics Laboratory. khara@pppl.gov
†Ph.D. Candidate, Princeton Plasma Physics Laboratory. skeller@pppl.gov
‡Principal Research Physicist, Princeton Plasma Physics Laboratory. Associate Fellow of AIAA. yraitses@pppl.gov

has been verified experimentally that the modulation in ion VDFs capture the discharge oscillations using a heterodyne approach.

II. Experiments: Cylindrical Hall thruster and Laser-induced fluorescence

The experiments are performed in a 2.6 cm cylindrical Hall thruster (CHT). The thruster was operated using xenon propellant with anode flow rate 2.5 sccm and cathode flow rate 1.5 sccm. The background pressure during thruster operation was about 5.1×10^{-5} Torr. The back magnetic coil current was 0.6 A and the front magnetic coil current was 1.27 A in "Direct" configuration. A 0.25 A keeper current was run between cathode emitter and keeper, together with a 12A heating current to stabilize the hollow cathode performance. When the discharge voltage was set to be 225 V, the thruster exhibits strong breathing oscillation at about 11.5 kHz. To couple with this natural oscillation, a 11.5 kHz square wave voltage between 210 V and 240 V was applied on thruster anode. The driven breathing mode was large and periodic as seen by the fast camera.

A. Forcing discharge voltage oscillation

The ion and discharge currents remain in phase for both natural and driven oscillations as shown in Figure 1.[12] The anode potential is set as

$$V(t) = V_D + \hat{V}\sin(\omega t), \tag{1}$$

where V_D is the DC component, $\hat{V}$ is the AC component, and ω is oscillation frequency. It can be seen that a breathing mode exists without any AC discharge voltage. At $\hat{V} = 3$ V, the discharge oscillation becomes slightly chaotic and again becomes coherent at $\hat{V} = 9$V. At a larger $\hat{V}$, *e.g.* $\hat{V} = 30$ V, the oscillation frequency remains unchanged while the amplitude increases. The phase alignment of ion and discharge currents suggests that driven and natural oscillations have similar physical mechanisms.

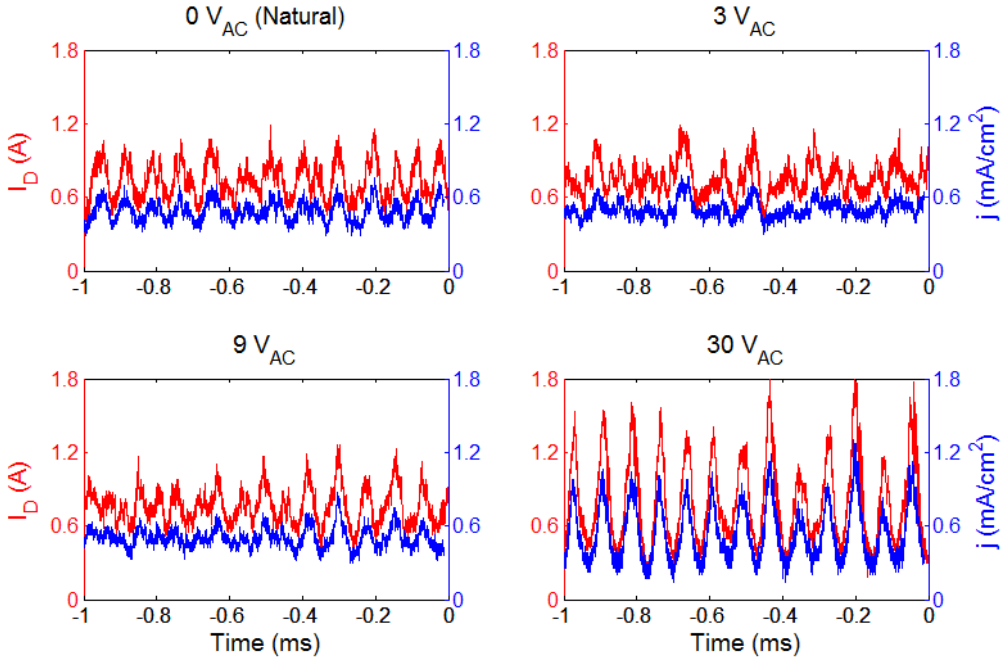

Figure 1. Discharge current oscillation and ion current oscillation obtained using a planar graphite probe with various oscillation amplitudes.[12]

B. Time-resolving laser-induced fluorescence

The ion velocity distribution function (IVDF) using LIF.[13] A tunable diode laser is used to pump the $5d^2F_{7/2}$ Xe^+ metastable level to $6p^2D^0_{5/2}$. The laser beam was aligned perpendicular to the thruster exit plane and

was injected into the thruster channel at along the thruster axis. The collection of LIF photons is performed 70 degrees with respect to the laser beam. The collected signal was detected using a photo-multiplier with an interference filter centered at 541 nm. A laser beam is chopped, typically at 100 kHz using an acousto-optic modulator (AOM), and directed along the thruster centerline.

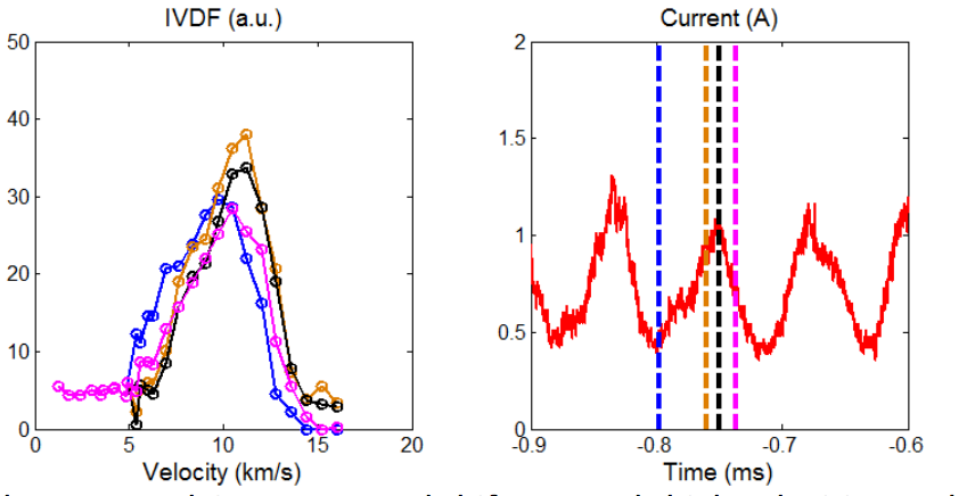

Figure 2. Large amplitude oscillation mode at $\hat{V} = 6$ V: Ion VDFs obtained from time-resolving LIF (on left), discharge current (on right). Reproduced from Ref. 12 and Ref. 13.

Figures 2 and 3 show the time-resolved results of IVDFs for different oscillation amplitude of the anode voltage. Figure 2 shows that the IVDFs are in-phase with the discharge current oscillation. The IVDF peak increases, and shifts towards high velocities as the discharge current (and voltage) increases. However, in Fig. 3, a collapse in the IVDF is observed at the peak of the current burst. Another study by Young et al.[14] indicates that the peak IVDF does not collapses but shifts to a much lower velocity.

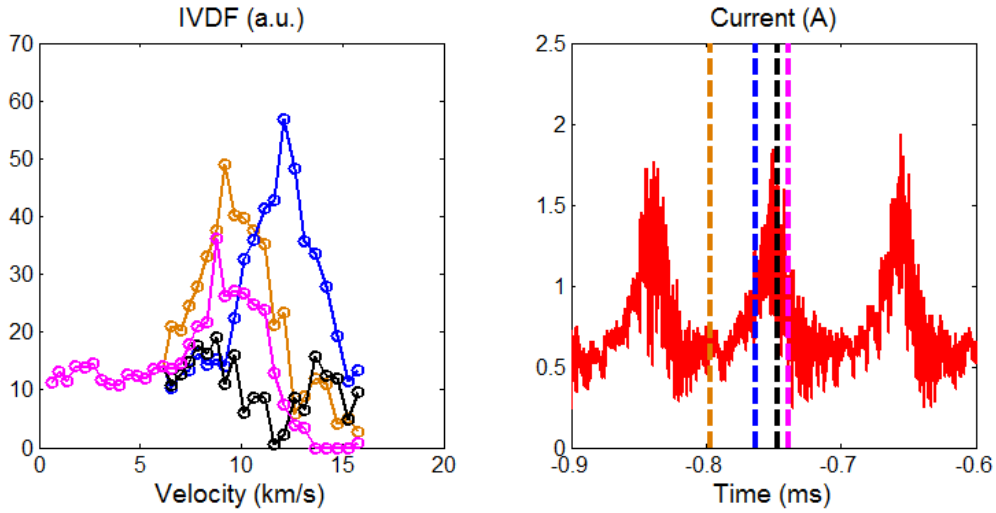

Figure 3. Large amplitude oscillation mode at $\hat{V} = 30$ V: Ion VDFs obtained from time-resolving LIF (on left), discharge current (on right). Reproduced from Ref. 12

III. Theory and Simulation: Low-frequency ionization oscillation

A. Predator-prey model

The predator-prey model assumes that the plasma is contained in an ionization box whose length is L and the spatial variation is neglected. The ionization rate coefficient ξ_{ion} and the velocities of ions and neutral atoms are constant in time. There is no ion flux entering the box and no neutral flux escaping the box. Using these assumptions, the continuity equations are written as

$$\frac{\partial N_i}{\partial t} + \frac{N_i U_i}{L} = N_i N_n \xi_{ion} \tag{2}$$

$$\frac{\partial N_n}{\partial t} - \frac{N_n U_n}{L} = -N_i N_n \xi_{ion}, \tag{3}$$

where N and U are the number density and mean velocity, and subscripts i and n denote ions and neutral atoms, respectively. To study the linear perturbation, a quantity follows the form: $Q = Q_0 + Q' \exp(-i\omega t)$, where Q_0 and Q' are equilibrium and perturbation quantities, respectively. From the first-order perturbation equation, the harmonic oscillator frequency can be obtained as

$$\omega = (N_{n,0} N_{i,0} \xi_{ion}^2)^{1/2}. \tag{4}$$

B. Ionization global model

A 0D global model of a plasma discharge is considered.[10] In order to construct a more accurate theory of ionization oscillations, the geometry is defined as shown in Ref. 10. The discharge plasma is assumed to be confined inside the discharge channel. Although the one-dimensional flow in the axial direction is of interest, the radial plasma diffusion also plays an important role. One can take an approach similar to a finite-volume method in which the state variables are volume averaged and the fluxes at interfaces are modeled. Without employing the undefined ionization length, ion and neutral continuity equations, ion momentum equation, and equations for electron momentum and energy are more correctly given by

$$\frac{\partial N_i}{\partial t} + \frac{N_i U_i}{L_{ch}} = N_i (N_n \xi_{ion} - \nu_{wl}) \tag{5}$$

$$\frac{\partial N_n}{\partial t} + \frac{(N_n - N_{int}) U_n}{L_{ch}} = -N_i (N_n \xi_{ion} - \nu_{wl}), \tag{6}$$

$$\frac{\partial U_i}{\partial t} + \frac{U_i^2}{L_{ch}} = \frac{e}{m_i} N_i E, \tag{7}$$

$$U_e = -\mu_\perp E, \tag{8}$$

$$\frac{\partial}{\partial t}\left(\frac{3}{2} N_i T_e\right) + \frac{5}{2} \frac{N_i U_i T_e}{L_c h} = S_{Joule} - S_{Wall} - S_{Coll}, \tag{9}$$

where N_{int} is the number density of neutral atoms at the anode that characterizes the anode mass inflow, $\nu_{wl} = 2U_{i,w}/R_\Delta$ is the ion loss frequency to the wall, $U_{i,w} = (eT_e/m_i)^{1/2}$ is the ion acoustic speed assuming that Bohm condition needs to be satisfied at the sheath edge in the vicinity of the channel walls, L_{ch} is the channel length, R_Δ is the channel width, U_e is the electron mean velocity, $\mu_\perp = \mu_0[1 + (\omega_B/\nu)^2]^{-1}$ is the effective electron mobility perpendicular to the magnetic field, $\mu_0 = e/(m_e\nu)$ is the electron mobility, $\omega_B = eB/m_e$ is gyrofrequency, and ν is the collision frequency. $S_{Joule} = -N_e U_e E$ is the Joule heating, $S_{Wall} = \nu_w \epsilon_w$ is the wall cooling contribution, where $\nu_w = 2\sqrt{eT_e/m_i}/R_\Delta/(1-\sigma)$, $\sigma = \max(0.986, T_e/25)$ is the secondary electron emission rate, $\epsilon_w = 2T_e + (1-\sigma)\phi_w$, and $\phi_w = -T_e \log[(1-\sigma)/\sqrt{2\pi m_e/m_i}]$ is the sheath potential; and $S_{Coll} = N_n \xi_{ion} \epsilon_i$, where $\epsilon_i = 12.1$ eV is the ionization energy for xenon. $\xi_{ion} = [AT_e^2 + B\log(-C/T_e)]\sqrt{8kT_e/\pi m_e}$, where $A = -1.0\times10^{24}$, $B = 6.386\times10^{-20}$, C = 12.13. The electron mean velocity, U_e, is assumed to be dependent only on the drift component as the diffusion component is typically negligible in the acceleration region. Any spatial variations are neglected inside the box due to the 0D assumption. A SPT-100 type thruster geometry is considered. In comparison to Ref. 10, the electron momentum treatment, i.e. Eq. 8, is added so that the modulation in electric field can be taken into consideration.

In this section, Eqs. 5 - 9 are solved by assuming that the electric field modulates:

$$E = \frac{V_d}{L}[1 + \alpha \sin(\omega_r t)], \tag{10}$$

where V_d is the mean discharge voltage, α is the oscillation strength, and ω_r is the oscillation frequency.

Figure 4 shows an example of the ionization oscillations with a modest oscillation strength, $\alpha = 0.05$. For a small perturbation, the oscillations are closer to a sinusoidal modulation, which exhibits a breathing mode oscillation. The phase between ion and neutral number density oscillations is approximately 90 degrees, see Figs. 4 (b) and (c). The electron temperature oscillates in a non-sinusoidal fashion as the electron temperature approaches the threshold value for space charge limited sheath, here $T_e \sim 25$ eV, and the wall heat flux of electrons increases due to S_{Wall} (Fig 4 (d)). However, the other quantities, such as ion mean velocity (e), electron mean velocity (f), and collision frequency (g), show a sinusoidal oscillation. Note that the time averaged ion mean velocity is approximately $\sim \sqrt{eV_d/m_i} = 12.7$ km/s. Finally, Fig. 4 (h) shows the discharge current calculated as $I_d = eN_i(U_i - U_e)A$, where A is the thruster area, and the ion current calculated as $I_i = eN_iU_iA$. Time is normalized by the oscillation frequency $\omega_r = 1.3 \times 10^4$ rad/s and two oscillation cycles are shown.

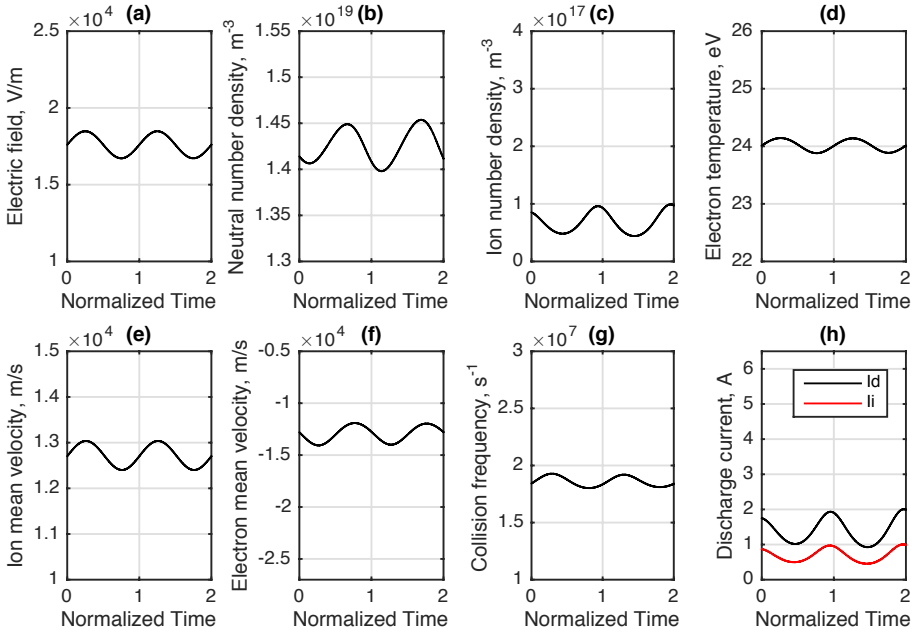

Figure 4. Modulation in the electric field is forced and the plasma response is shown. (a) Electric field, (b) neutral atom density, (c) ion density, (d) electron temperature, (e) ion mean velocity, (f) electron mean velocity, (g) collision frequency, and (h) discharge and ion current. Oscillation strength is $\alpha = 0.05$.

The ion density and discharge current are in-phase as the current strongly depends on the ion number density. At the same time, the electric field, electron temperature, and ion mean velocity are also in-phase because the Joule heating strongly drives the electron temperature oscillation as shown in Eq. 9 and the ion momentum depends almost only on the electric field as can be seen from Eq. 7. The electric field and electron mean velocity is 180 degrees out-of-phase, see Eq. 8. Phase difference can be seen from the ion and neutral continuity equation (Eqs. 5 and 6). Here, in order to investigate the phase shift between the ion and neutral density vs. the electron temperature, assume that the radial loss component is negligible, $\nu_{wl} = 0$ and a forced oscillation in the ionization rate coefficient to follow $\xi_{ion} = \xi_0[1 + \alpha_0 \cos(\omega_r t)]$. The linear perturbation equations can be written as

$$\frac{\partial^2 N_i'}{\partial t^2} + \nu_d \frac{\partial N_i'}{\partial t} + \omega_0^2 N_i' = \alpha_0 \omega_0^2 \left[\frac{N_{n0}}{N_{int} - N_{n0}} \cos(\omega_r t) - \frac{\omega_r}{\xi_0} \sin(\omega_r t) \right] \tag{11}$$

$$\frac{\partial^2 N_n'}{\partial t^2} + \nu_d \frac{\partial N_n'}{\partial t} + \omega_0^2 N_n' = \alpha_0 \omega_0^2 \left[-N_{n0} \cos(\omega_r t) + \frac{\omega_r}{\xi_0} \sin(\omega_r t) \right] \tag{12}$$

where $\nu_d = (N_{int}/N_{n0})U_n/L_{ch}$ is the damping frequency due to the constant neutral atom inflow from the anode and ω_0 is the natural frequency obtained in Eq. 4. These equations are general ordinary differential equations (ODEs) with damping, natural oscillation, and forced oscillation terms. The solution to the two perturbation equations give the amplitude and phase of the oscillation. For a general ODE,

$$\ddot{x} + \nu_d \dot{x} + \omega_0^2 x = \omega_0^2 X_0 \cos(\omega_r t) + \omega_0^2 Y_0 \sin(\omega_r t), \tag{13}$$

the amplitude and phase can be obtained as

$$x_0 = \frac{\omega_0^2}{\sqrt{(\omega_0^2 - \omega_r^2)^2 + (\nu\omega_r)^2}} \sqrt{X_0^2 + Y_0^2} \tag{14}$$

$$\tan\phi = \frac{X_0 \nu\omega_r + Y_0(\omega_0^2 - \omega_r^2)}{X_0(\omega_0^2 - \omega_r^2) - Y_0 \nu\omega_r}. \tag{15}$$

One immediate observation from Eq. 14 is that the resonant oscillation $x_0 \to \infty$ occurs when the forcing frequency ω_r is equal to the natural frequency ω_0 and the damping frequency is zero. It is also apparent that x_0 will not be infinite even for $\omega_r = \omega_0$ because $\nu_d \neq 0$ in actual Hall thruster systems. Then, from Eqs. 11 and 12, the phase of the ion and neutral atom density oscillations with respect to the forced oscillation in the ionization rate coefficient can be given as

$$\tan(\phi_i) = -\frac{N_{n0}}{N_{int} - N_{n0}} \sqrt{\frac{N_{i0}}{N_{n0}}} \tag{16}$$

$$\tan(\phi_n) = -\sqrt{\frac{N_{n0}}{N_{i0}}}. \tag{17}$$

In the limit of $N_{i0} \ll N_{n0}$, the ion density oscillation is perfectly in phase with the ionization rate coefficient and the neutral density oscillation is 90 degrees out of phase.

In Fig. 4. since it is likely that ω_r that was chosen is not equal to ω_0, there can be additional phase difference between the density profiles and the ionization rate coefficient, which is dependent on the electron temperature. In the experiments as shown in Fig. 2, the discharge current oscillation is almost in-phase with the ion VDF measurements. The phase differences can be attributed to such differences in the selection of driving oscillation frequency and the plasma properties. Ref. 14 also shows that there is phase shift between the ion VDF contours and the discharge current oscillation.

Figure 5 shows the results for a larger oscillation amplitude, $\alpha = 0.3$. All quantities except for the forced electric field exhibit non-sinusoidal oscillations. The phase of the plasma properties is almost identical to the small oscillation amplitude case, shown in Fig. 4. The non-sinusoidal profile is a result of the higher order terms being important whereas the sinusoidal profile is indicative of a linear perturbation. As shown in Fig. 5 (d), the electron temperature is noisy as it approaches the threshold value $T_e \sim 25$ eV. This leads to some high frequency oscillations in ion mean velocity (e), electron mean velocity (f), collision frequency (g), and discharge current (h). The most interesting observation here is the ion mean velocity oscillation. The ion mean velocity oscillates in-phase with the electric field oscillation. This indicates that the shift in IVDFs to a lower velocity, if any, from the LIF measurements can be due to the rapid change in electric field and that the ion mean velocity is strongly dependent on the electric field.

C. 1D Hybrid Simulation Result

The shift in the IVDFs to a lower velocity is also observed in hybrid simulations where a kinetic method is used for ions and a fluid model is used for electrons. The model is described in Ref. 15. Here, a simplified electron fluid model is used and no anomalous mobility is assumed. The anode is $x = 0$ cm and the channel exit is $x = 4$ cm.

In Ref. 15, a particle-in-cell (PIC) simulation and a direct kinetic (DK) simulation were used for ions and compared while an identical fluid model is used for electrons. In the DK simulation, kinetic equations, such as the Vlasov and/or Boltzmann equations, are solved directly in discretized phase space rather than assuming computational macroparticles as for the PIC simulation. Two kinetic methods were benchmarked and the macroscopic quantities were similar but the plasma oscillations were observed without any statistical noise in the hybrid-DK simulation.

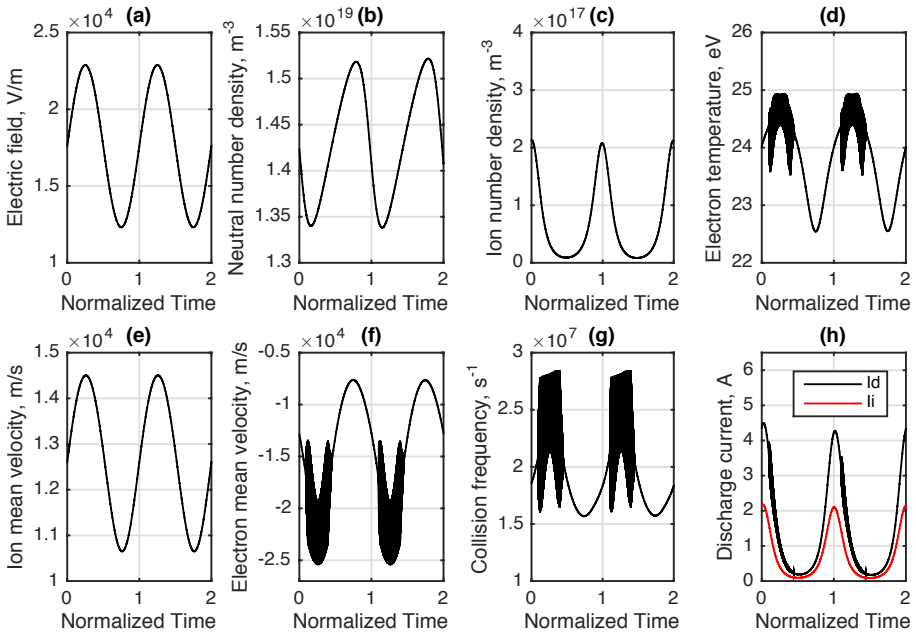

Figure 5. The plasma response to a forced electric field modulation is shown similar to Fig. 4. Oscillation strength is $\alpha = 0.3$.

Figure 6 shows the time evolution of the ion VDFs as well as the discharge current oscillation. A breathing mode type oscillation is observed throughout the simulation. The ions are accelerated in the channel and escapes from the channel exit most of the time. However, as shown in Fig. 6 (a), there is a peculiar mode, where slow ions stay in the acceleration region. Note that this is not a numerical artifact due to the DK solver as a similar phenomenon are observed using the PIC simulation. The slow ion blob occurs when the ion current exceeds the discharge current in the channel. This is because the electron current becomes negative ($j_e = -eN_eU_e \approx eN_e\mu E < 0$) and the electric field will be reversed ($E < 0$). The locally reversed electric field will slow down the ions and accumulate ions. It can be seen from Fig. 6 (a) that the slow ions are dominant but there are still streaming ions ($\sim 21,000$ m/s) that are generated in the ionization region inside the channel. These double peaked ion VDFs were observed in Young's LIF measurements.[14]

The corresponding time evolution of the electric field and electron mean energy are shown in Fig. 7. Except for the time when the slow ion VDFs are observed (Fig. 6(a)), the electric field and electron mean energy are relatively unchanged. As can be seen from Fig. 7(a), the slow ion VDFs near the channel exit are supported by the reversed electric field. The large electric field generated behind the slow ion region also result in large electron heating due to Joule heating, leading to a local region where electron energy is large as shown in Fig. 7(b). The numerical results suggest that it is possible in the cylindrical Hall thruster that a reversed electric field is generated locally, which could cause slow moving ions either towards the exit or back inside the channel. Another possibility is that the electron mean energy or temperature decreases rapidly that results in a change in the electron energy distribution function and loss of the excited ion species, from which the LIF signal is obtained. The 2D structure of the plasma properties must be measured carefully in experiments and calculated using high-fidelity numerical simulations that can take into account the complex magnetic field structure of the cylindrical Hall thrusters.

IV. Conclusion

Time-resolving laser-induced fluorescence technique has been developed to investigate the ion velocity distribution functions in a cylindrical Hall thruster. Ion measurements are useful to understand the oscillation mechanism of the discharge plasma in a Hall thruster. A collapse in the distribution functions is observed in a nonlinear oscillation mode where strong discharge oscillations are excited.

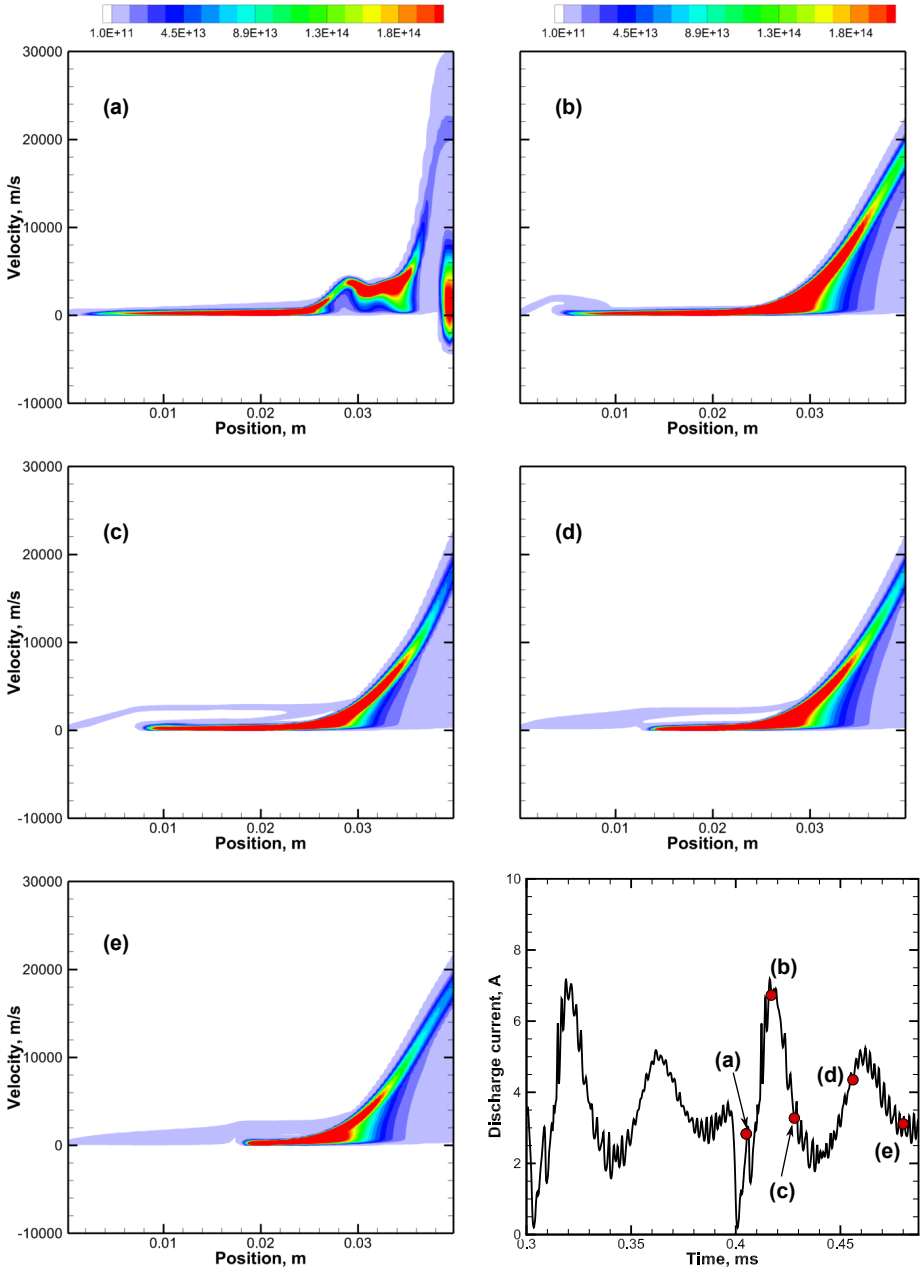

Figure 6. Hybrid-DK simulation of a SPT-100 type Hall thruster. The bottom right is the discharge current oscillation and the ion VDFs for the corresponding timesteps are shown from (a) to (e). Reproduced from Ref. 16.

A global ionization model, which is a zero-dimensional transport model, is developed and used to investigate the stabilization and excitation of ionization oscillations. Phase and amplitude of the linear and nonlinear modes can be obtained from the theory and will be compared to experiments. The results obtained from the global ionization model show that the ion mean velocity can decrease during the discharge oscillation, which suggests that the ion distribution function will shift to a smaller velocity. Another possibility is a dynamic oscillation inside the channel where reversed electric field is generated locally. This will create a very slow moving ion bunch or even ions that move back inside the channel.

More detailed experimental investigations are needed including spatially and temporally mapping the time-resolved IVDFs and ion currents. We also plan to employ high fidelity electron fluid models that

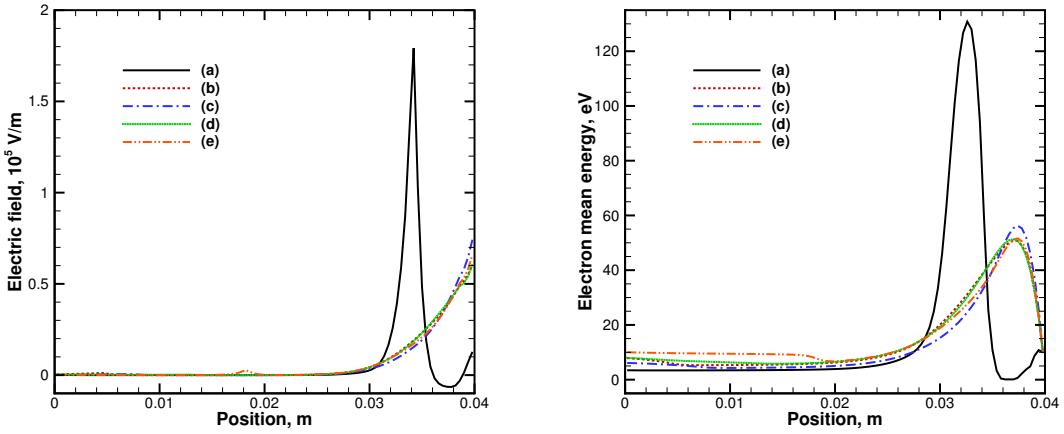

(a) Electric field

(b) Electron mean energy

Figure 7. Hybrid-DK simulation of a SPT-100 type Hall thruster. The timesteps correspond to those shown in Fig. 6

accounts for multidimensional structure of the magnetic field[17,18] in order to investigate discharge oscillations in the cylindrical Hall thruster.

Acknowledgement

The experimental work conducted at PPPL is supported by AFOSR and US Department of Energy. The first author thanks the Japan Society for the Promotion of Science for financial support. The authors acknowledge Dr. Ahmed Diallo for experimental assistance.

References

[1]Tilinin, G. N., "High-frequency plasma waves in a Hall accelerator with an extended acceleration zone," *Sov. Phys. Tech. Phys.*, Vol. 22, 1977, pp. 974–978.

[2]Gascon, N., Dudeck, M., and Barral, S., "Wall material effects in stationary plasma thrusters. I. Parametric studies of an SPT-100," *Physics of Plasmas*, Vol. 10, No. 10, 2003, pp. 4123–4136.

[3]Brown, D. L., Larson, C. W., Beal, B. E., and Gallimore, A. D., "Methodology and Historical Perspective of a Hall Thruster Efficiency Analysis," *Journal of Propulsion and Power*, Vol. 25, No. 6, November 2009, pp. 1163–1177.

[4]Sekerak, M. J., Longmier, B. W., Gallimore, A. D., Brown, D. L., Hofer, R. R., and Polk, J. E., "Mode Transitions in Hall Effect Thrusters," AIAA 2013-4116, San Jose, CA, July 2013.

[5]Fife, J. M., *Hybrid-PIC Modeling and Electrostatic Probe Survey of Hall Thrusters*, Ph.D. thesis, MIT, 1998.

[6]Bareilles, J., Hagelaar, G. J. M., Garrigues, L., Boniface, C., Boeuf, J. P., and Gascon, N., "Critical assessment of a two-dimensional hybrid Hall thruster model: Comparisons with experiments," *Physics of Plasmas*, Vol. 11, No. 6, June 2004, pp. 3035–3046.

[7]Barral, S. and Ahedo, E., "On the Origin of Low Frequency Oscillations in Hall Thrusters," *AIP Conference Proceedings*, Vol. 993, 2008, pp. 439–442.

[8]Barral, S. and Ahedo, E., "Low-frequency model of breathing oscillations in Hall discharges," *Phys. Rev. E*, Vol. 79, Apr 2009, pp. 046401.

[9]Hara, K., Sekerak, M. J., Boyd, I. D., and Gallimore, A. D., "Mode transition of a Hall thruster discharge plasma," *Journal of Applied Physics*, Vol. 115, No. 20, 2014.

[10]Hara, K., Sekerak, M. J., Boyd, I. D., and Gallimore, A. D., "Perturbation analysis of ionization oscillations in Hall effect thrusters," *Physics of Plasmas (1994-present)*, Vol. 21, No. 12, 2014.

[11]Diallo, A., Shi, Y., Keller, S., Raitses, Y., and Mazouffre, S., "Time-Dependent Ion Velocity Distribution: A novel Heterodyne Laser-Induced Fluorescence with Coupled Wave Excitation," IEPC-2013-239, Washington, D.C., USA, October 2013.

[12]Keller, S., Diallo, A., and Raitses, Y., "Laser-induced fluorescence measurements of driven breathing oscillations in a Hall thruster," New Orleans, LA, November 2014.

[13]Diallo, A., Shi, Y., Keller, S., Raitses, Y., and Mazouffre, S., "Time-resolved ion velocity distribution in a cylindrical Hall thruster: Heterodyne-based experiment and modeling," *Review of Scientific Measurements*, Vol. 86, 2015, pp. 033506.

[14]Young, C. V., Lucca Fabris, A., and Cappelli, M. A., "Ion dynamics in an EâĂĽÃŮâĂĽB Hall plasma accelerator," *Applied Physics Letters*, Vol. 106, No. 4, 2015, pp. –.

[15]Hara, K., Boyd, I. D., and Kolobov, V. I., "One-dimensional hybrid-direct kinetic simulation of the discharge plasma in a Hall thruster," *Physics of Plasmas*, Vol. 19, No. 11, 2012.

[16]Hara, K., *Development of Grid-Based Direct Kinetic Method and Hybrid Kinetic-Continuum Modeling of Hall Thruster Discharge Plasmas*, Ph.D. thesis, University of Michigan, 2015.

[17]Kawashima, R., Komurasaki, K., and Schronherr, T., "A hyperbolic-equation system approach for magnetized electron fluids in quasi-neutral plasmas," *Journal of Computational Physics*, Vol. 284, 2015, pp. 59 – 69.

[18]Dragnea, H. C., Hara, K., and Boyd, I. D., "Fully 2D Numerical Simulation of a Nested Channel Hall Thruster," SP2016 3124969, Rome, Italy, May 2016.